THE JOURNAL OF PHYSICAL CHEMISTRY B

Article

pubs.acs.org/JPCB

Pyroglutamylated Amyloid-β Peptide Reverses Cross β-Sheets by a Prion-Like Mechanism

Jason O. Matos,[†,‡] Greg Goldblatt,[§,‡] Jaekyun Jeon,[∥,‡] Bo Chen,[‡] and Suren A. Tatulian*[,‡]

[†]Biotechnology Graduate Program, University of Central Florida, 4000 Central Florida Boulevard, Orlando, Florida 32816, United States

[‡]Department of Physics, University of Central Florida, 4000 Central Florida Boulevard, Orlando, Florida 32816, United States

[§]Biomedical Sciences Graduate Program, University of Central Florida, 4000 Central Florida Boulevard, Orlando, Florida 32816, United States

[∥]Physics Graduate Program, University of Central Florida, 4000 Central Florida Boulevard, Orlando, Florida 32816, United States

ABSTRACT: The amyloid hypothesis causatively relates the fibrillar deposits of amyloid β peptide (Aβ) to Alzheimer's disease (AD). More recent data, however, identify the soluble oligomers as the major cytotoxic entities. Pyroglutamylated Aβ (pE-Aβ) is present in AD brains and exerts augmented neurotoxicity, which is believed to result from its higher β-sheet propensity and faster fibrillization. While this concept is based on a set of experimental results, others have reported similar β-sheet contents in unmodified and pyroglutamylated Aβ, and slower aggregation of pE-Aβ as compared to unmodified Aβ, leaving the issue unresolved. Here, we assess the structural differences between Aβ and pE-Aβ peptides that may underlie their distinct cytotoxicities. Transmission electron microscopy identifies a larger number of prefibrillar aggregates of pE-Aβ at early stages of aggregation and suggests that pE-Aβ affects the fibrillogenesis even at low molar fractions. Circular dichroism and FTIR data indicate that while the unmodified Aβ readily forms β-sheet fibrils in aqueous media, pE-Aβ displays increased α-helical and decreased β-sheet propensity. Moreover, isotope-edited FTIR spectroscopy shows that pE-Aβ reverses β-sheet formation and hence fibrillogenesis of the unmodified Aβ peptide via a prion-like mechanism. These data provide a novel structural mechanism for pE-Aβ hypertoxicity; pE-Aβ undergoes faster formation of prefibrillar aggregates due to its increased hydrophobicity, thus shifting the initial stages of fibrillogenesis toward smaller, hypertoxic oligomers of partial α-helical structure.

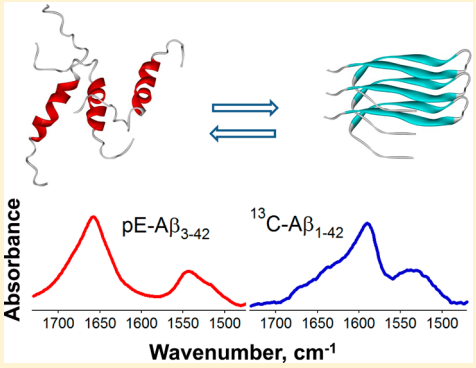

1. INTRODUCTION

Alzheimer's disease (AD) is a neurodegenerative disorder characterized by neuronal and synaptic loss leading to cognitive and memory impairment. Extracellular fibrillar deposits (plaques) of amyloid-β (Aβ) peptide have been found in the AD brain and thought to be causatively related to the disease.[1−3] However, currently accumulated evidence identifies the soluble oligomers of Aβ as the main neurotoxic entities.[4−8]

Aβ is a proteolytic product of the amyloid precursor protein and can contain varying numbers of amino acid residues, with the 40- and 42-residue peptides ($A\beta_{1-40}$ and $A\beta_{1-42}$) being the prevalent forms. Circular dichroism (CD) and NMR data indicate that in organic solvents such as hexafluoroisopropanol (HFIP) $A\beta_{1-42}$ adopts a partially α-helical structure and in the presence of >80% H_2O acquires a β-sheet structure.[9] In aqueous media, Aβ forms fibrils composed of β-sheets where the strand axis is approximately perpendicular and the H-bonding is parallel to the long fibrillar axis, known as a cross β-sheet structure.[10,11] Antiparallel β-sheets were proposed to constitute the core structural motif of fibrils formed by $A\beta_{1-42}$ or its fragments.[12,13] However, solid state NMR studies on $A\beta_{1-42}$ and shorter peptides identified in-register parallel β-sheet structures,[14−16] consistent with models derived from spin-label EPR,[17] solution NMR,[18] and Fourier transform infrared (FTIR) studies.[19,20] Apparent inconsistencies might originate from different stages of peptide aggregation in different samples, as $A\beta_{1-42}$ oligomers and fibrils were shown by FTIR to adopt antiparallel and parallel β-sheet structures, respectively.[21]

Significant amounts of N-terminally truncated and pyroglutamylated (at Glu3 or Glu11) Aβ peptide (pE-Aβ) have been identified in AD brains and shown to aggregate at increased rates[22−26] and to be more cytotoxic than unmodified Aβ.[27,28] Even at low fractions, pE-Aβ coaggregates with Aβ by a seeding mechanism and forms structurally distinct and highly toxic oligomers.[27] Dot-blot experiments using conformation-sensitive antibodies showed that the highly toxic oligomers containing 5% or less pE-Aβ were structurally different from the mildly toxic unmodified Aβ aggregates of similar size.[27] While these studies imply a structural mechanism for augmented toxicity of

Received: December 29, 2013
Revised: May 6, 2014
Published: May 6, 2014

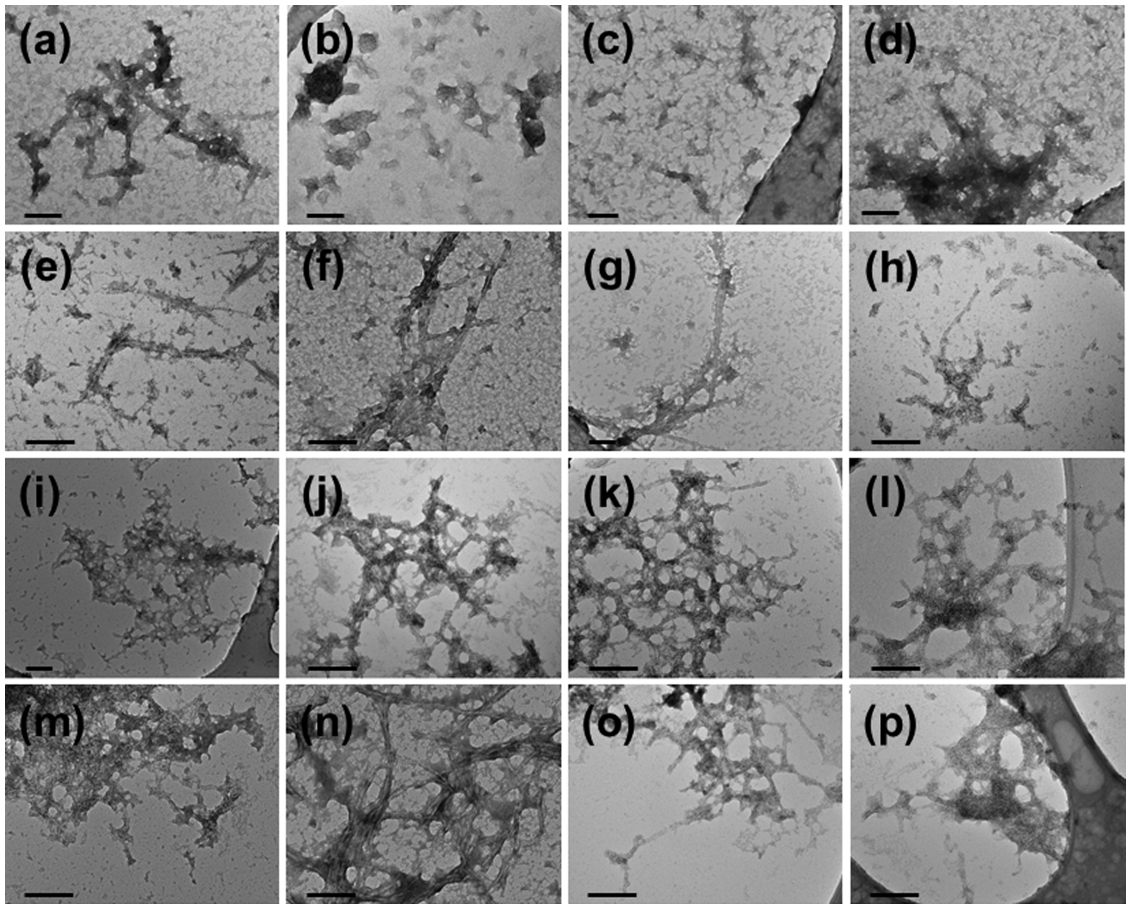

Figure 1. TEM images of $A\beta_{1-42}$ (a, e, i, m), $A\beta_{pE3-42}$ (b, f, j, n), $A\beta_{pE3-42}/A\beta_{1-42}$ = 1:9 (c, g, k, o), and $A\beta_{pE3-42}/A\beta_{1-42}$ = 1:1 (d, h, l, p) incubated in aqueous buffer of 50 mM NaCl + 50 mM Na,K-phosphate (pH 7.2) for 2 h (a–d), 4 h (e–h), 12 h (i–l), and 24 h (m–p) at 37 °C with constant stirring. The horizontal bar in each panel equals 100 nm.

pE-Aβ, the underlying structural differences between Aβ and pE-Aβ remain uncharacterized. Solution NMR showed that $A\beta_{pE3-40}$ in trifuoroethanol/water (2:3) has a reduced α-helical propensity compared to $A\beta_{1-40}$,[29] consistent with a significantly higher β-sheet content and faster fibrillogenesis of pE-Aβ.[23,25] Conversely, CD studies identified similar content of β-sheet in both unmodified Aβ and pE-Aβ peptides,[30] and fibrillogenesis of $A\beta_{pE3-42}$ was reported to be significantly slower compared to $A\beta_{1-42}$.[31] These conflicting data on fibrillogenesis of unmodified Aβ and pE-Aβ are evidently related to the inherent polymorphism and sensitivity of the Aβ peptides to the experimental conditions and procedures.[32,33] Since the content of pE-Aβ in AD brains varies in a wide range and affects the structure and the toxicity of the amyloid aggregates,[27,34,35] individual structures of unmodified Aβ and pE-Aβ separately and in combination, as well as the mutual structural effects, should be determined to shed light on the molecular mechanism underlying the altered fibrillogenesis of pE-Aβ.

Here, we have employed transmission electron microscopy (TEM), CD, and FTIR spectroscopy to analyze structural transitions in $A\beta_{1-42}$ and $A\beta_{pE3-42}$ peptides during fibrillogenesis. Isotope-edited FTIR was used to examine structural changes in both peptides combined in one sample, which allowed identification of the profound prion-like conformational effect of pE-Aβ on the unmodified Aβ. Specifically, pE-Aβ not only exhibited an increased α-helical and reduced β-sheet propensity but also was able to retard β-sheet formation by Aβ and to reverse β-sheets to α-helical structure at initial stages of fibrillogenesis. These findings suggest that the augmented cytotoxicity of pE-Aβ may result from its preference to form hypertoxic aggregates of partial α-helical structure as opposed to mildly toxic β-sheet fibrils.

2. MATERIALS AND METHODS

Materials. The $A\beta_{1-42}$ and uniformly ^{13}C-labeled $A\beta_{1-42}$ peptides were purchased from rPeptide (Bogart, GA, USA) and were >97% pure. $A\beta_{pE3-42}$ was from Innovagen (Lund, Sweden) and was 98% pure. The peptides were analyzed by MALDI-TOF mass-spectrometry at the ICBR Proteomics Core Facility of the University of Florida (Gainesville, FL, USA), and the amino acid compositions of all three peptides were confirmed. Salts, buffers, HFIP, and other chemicals were from Fisher Scientific (Hanover Park, IL, USA) or Sigma-Aldrich (St. Louis, MO, USA).

Experimental Procedures. In all experiments, the lyophilized peptides were initially dissolved in HFIP at 200 μM concentration to disperse any preformed aggregates. In TEM experiments, appropriate amounts of the peptides were dried in a glass vial by desiccation for 15 min, followed by incubation in an aqueous buffer of 50 mM NaCl + 50 mM Na,K-phosphate (pH 7.2) at 37 °C with constant stirring for 24 h. TEM samples were prepared following the procedures described by Nilsson,[36] i.e., by deposition of 5 μL of peptide suspension on the grid, incubation for 5 min, and rinsing with 4 μL of distilled/deionized water, followed by staining for 30 s

dx.doi.org/10.1021/jp412743s | J. Phys. Chem. B 2014, 118, 5637–5643

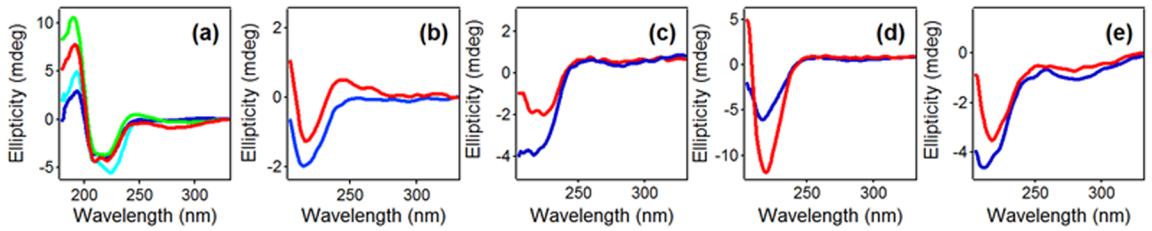

Figure 2. CD spectra of dry and water-suspended peptides. (a) $A\beta_{1\text{-}42}$ (green), $A\beta_{pE3\text{-}42}$ (turquoise), $A\beta_{pE3\text{-}42}/A\beta_{1-42}$ = 1:9 (blue), and $A\beta_{pE3\text{-}42}/A\beta_{1-42}$ = 1:1 (red) were dissolved in HFIP, followed by 15 min of desiccation in a 4 mm × 4 mm quartz cuvette and collection of the spectra. (b–e) Aqueous buffer of 50 mM NaCl + 50 mM Na,K-phosphate (pH 7.2) was added to a 50 μM final concentration of $A\beta_{1-42}$ (b), $A\beta_{pE3\text{-}42}$ (c), $A\beta_{pE3\text{-}42}/A\beta_{1-42}$ = 1:9 (d), and $A\beta_{pE3\text{-}42}/A\beta_{1-42}$ = 1:1 (e), and spectra were acquired after 1 h (blue) and 24 h (red) of incubation at 37 °C with constant stirring.

with 2 μL of 3% uranyl acetate, washing twice with 5 μL of distilled/deionized water, and air-drying. Grids for the negative control experiments were prepared by identical procedures using 5 μL of blank buffer instead of the peptide suspension. Images were acquired on a JEOL TEM-1011 operated at 80 kV using thin (<3 nm) holey carbon grids (Ted Pella, Inc., Redding, CA, USA).

In CD experiments, the HFIP solutions of peptides were dried by desiccation in a 4 mm × 4 mm quartz cuvette and spectra were collected between 180 and 330 nm to determine the structure of the dry peptides. Subsequently, an aqueous buffer of 50 mM NaCl + 50 mM Na,K-phosphate (pH 7.2) was added to a 50 μM final concentration of the peptides and spectra were acquired consecutively for 24 h to identify secondary structural changes upon fibrillogenesis at 37 °C with constant stirring, using a J-810 spectropolarimeter (Jasco, Tokyo, Japan). To improve the signal-to-noise ratio, the spectra were smoothed using a 13-point Savitzky-Golay linear least-squares algorithm embedded in the Igor Pro 5.03 software.

FTIR experiments were conducted to determine the structure of the peptides in desiccated form, nominally hydrated by atmospheric humidity, and in the presence of excess aqueous buffer. Desired amounts of the peptides were dissolved in HFIP at 200 μM concentration, and 40 μL of the solution was placed on a CaF_2 FTIR window and dried in a desiccator for 15 min. FTIR spectra of the peptide samples were collected while the peptide was allowed to absorb humidity from the atmosphere as monitored by the increase in the H_2O stretching band intensity around 3270 cm^{-1}. Then, 80 μL of aqueous buffer (10 mM Na,K-phosphate in D_2O, pD 7.2, corresponding to the pH-meter reading of 6.8) was added to the peptide and the sample was sealed by a second window using a 50 μm-thick Teflon spacer, followed by measurements of spectra of the peptide in aqueous medium. The spectra were measured by coadding 500 scans on a Vector-22 FTIR spectrometer (Bruker Optics, Billerica, MA, USA) equipped with a liquid nitrogen-cooled Hg–Cd–Te detector, at 2 cm^{-1} nominal resolution at 25 °C, as described earlier.[37] Reference transmission spectra were collected using either a single CaF_2 window or the buffer sealed between two windows and were used to calculate the absorbance spectra. H_2O vapor spectra were measured separately and subtracted from the sample spectra when necessary. The spectra were smoothed as described above, and baseline correction was applied.

3. RESULTS

Based on earlier findings that $A\beta_{pE3\text{-}42}$ forms aggregates that are structurally different from the aggregates of $A\beta_{1-42}$ and exert prion-like toxicity on cultured neurons,[27] we hypothesized that $A\beta_{pE3\text{-}42}$ modulates the structure of the unmodified peptide reminiscent of prions. Since the content of pyroglutamylated $A\beta$ can vary up to 50% of total $A\beta$,[27,34,35] we studied pE-$A\beta$/$A\beta$ samples at 1:9 and 1:1 molar ratios in addition to pure $A\beta$ and pE-$A\beta$ peptides. TEM images were acquired at 2, 4, 12, and 24 h of incubation, as described in the Materials and Methods. Most significant differences between $A\beta_{1-42}$ and $A\beta_{pE3\text{-}42}$ were detected at the early stages of aggregation. At 2 h, the samples of $A\beta_{pE3\text{-}42}$ were dominated by nonfibrillar aggregates of irregular shape and average dimension of 30–100 nm, while the $A\beta_{1-42}$ samples showed well-defined fibrils and a smaller number of small aggregates (Figure 1a and b). The 1:9 and 1:1 molar combinations contained predominantly prefibrillar structures (Figure 1c and d). At 4 h of incubation, the fibrils were seen in all samples, with little morphological differences, with small aggregates still present (Figure 1e–h). With progression of fibrillogenesis through 24 h, the small aggregates were converted to fibrils which became more extended and entangled (Figure 1i–p). While the mature fibrils formed by the $A\beta_{pE3\text{-}42}$ peptide seem to be thicker, possibly bundled (cf. part n of Figure 1 with parts m, o, and p), consistent with earlier observations,[24,28] the TEM data do not allow identification of more distinct, definitive morphological differences between the fibrils of the unmodified and pyroglutamylated peptides and their combinations. Taking into account the clear differences between the early stage assemblies of $A\beta_{1-42}$ and $A\beta_{pE3\text{-}42}$, these data suggest that the fibrillogenesis of the two forms may follow different pathways, leading to fibrils that are similar at the level of morphology. The images obtained in negative control experiments showed clear grids, as expected (not shown).

Earlier TEM studies showed similar morphologies of $A\beta_{pE3\text{-}42}$ and $A\beta_{1-42}$ aggregates at the initial stages of aggregation but more "curvilinear and entangled" fibrils of $A\beta_{1-42}$ at 1–2 days of fibrillogenesis.[38,39] In the equimolar sample, the fibrils were less entangled, i.e. more like $A\beta_{pE3\text{-}42}$ fibrils, suggesting that pE-$A\beta$ might be able to dictate its morphological (and probably structural) features to the aggregates.

It has been recognized that the fibrillar morphology is determined by the molecular structure of the peptides,[23,30,38,39] but CD studies provided conflicting data on the relative secondary structural changes in $A\beta$ and pE-$A\beta$ during fibrillogenesis (see above). To monitor the structural transitions in the peptides during fibrillogenesis, peptide samples dried from HFIP solution were used as a starting point, before the onset of aggregation. CD spectra of $A\beta_{1-42}$, $A\beta_{pE3\text{-}42}$, and their combinations in dry form shown in Figure 2a indicate mostly α-helical structure with two minima around 222 and 208 nm.[40,41] The spectrum of $A\beta_{pE3\text{-}42}$ has a significantly

dx.doi.org/10.1021/jp412743s | J. Phys. Chem. B 2014, 118, 5637–5643

reduced ratio of ellipticities $\theta_{208}/\theta_{222}$, indicative of a more flexible or disordered α-helix.[42] These results concur with solution NMR data showing α-helical conformation for both $A\beta_{1-42}$ and $A\beta_{pE3-40}$ in organic solvents.[9,29] Upon addition of an aqueous buffer and incubation at 37 °C with constant stirring, the peptides undergo significant structural changes. $A\beta_{1-42}$ promptly adopts and maintains β-sheet structure, as evidenced by a deep minimum at 215−216 nm of spectra measured at 1 and 24 h of incubation (Figure 2b). The spectra of $A\beta_{pE3-42}$, on the other hand, show a wide well between 208 and 222 nm, most likely indicating a combination of α-helical and β-sheet structures (Figure 2c). These data suggest substantially different structures of $A\beta_{1-42}$ and $A\beta_{pE3-42}$, while the former readily adopts β-sheets, the latter shows increased α-helical propensity. The CD spectra of the 1:9 $A\beta_{pE3-42}/A\beta_{1-42}$ combination display β-sheet features, i.e. a prominent minimum at 216 nm at 1 h and at 219 nm at 24 h of incubation (Figure 2d). The higher intensity and the red shift of the signal at 24 h may reflect gradual suspension of the peptide into the aqueous medium and decreased solvent accessibility upon aggregation.[40] It should be noted that the spectra of Figure 2d are dominated by the structural features of $A\beta_{1-42}$ which are present at a large molar excess (90%). At 1:1 molar ratio, the 1-h spectrum shows a minimum at 209 and a shoulder at 223 nm (Figure 2e), implying α-helix structure, possibly including a β-sheet component, as in the case of pure $A\beta_{pE3-42}$ (cf. blue spectra in Figure 2c and e). At 24 h, the spectrum has a β-sheet minimum at 216 nm and a shoulder at 227 nm, likely generated by a turn structure. It is remarkable that $A\beta_{pE3-42}$ exerts a dominant structural effect, especially at the early stages of fibrillogenesis. Thus, consistent with the TEM data, CD results indicate that (a) $A\beta_{1-42}$ and $A\beta_{pE3-42}$ evidently follow distinct structural pathways of fibrillogenesis and (b) $A\beta_{pE3-42}$ is able to divert the overall path toward less β-sheet and more α-helical intermediates.

While TEM and CD data indicate distinct structural differences between $A\beta_{1-42}$ and $A\beta_{pE3-42}$ and suggest a dominant structural effect of pE-Aβ on Aβ, neither of these methods has the capability of resolving the individual structures of the two peptides in combination and the mutual structural effects. Individual structures of two proteins combined in one sample can be determined by FTIR spectroscopy if their amide I bands are spectrally separated, which is achieved by ^{13}C-labeling of one of the proteins.[43−45] Despite its resolving power, such "isotope-edited" FTIR spectroscopy has not been used to characterize the concomitant structural transitions of Aβ and pE-Aβ during fibrillogenesis.

To detect the structural changes accompanying formation of amyloid fibrils, FTIR spectra were measured before and after exposure of the peptides to an aqueous buffer. Both peptides were dissolved in HFIP and dried on a CaF_2 window by 15 min desiccation. $A\beta_{pE3-42}$ adopts an intramolecular antiparallel β-sheet structure (peak at 1634 cm^{-1} and shoulder around 1695 cm^{-1}), as well as a significant fraction of α-helix and turn structures (broad component(s) between 1685 and 1650 cm^{-1}) (Figure 3a).[45−47] ^{13}C-$A\beta_{1-42}$ forms an intermolecular β-sheet (main peak at 1588 cm^{-1}) plus turns and an insignificant α-helix (component at 1617 cm^{-1}) (Figure 3a). These data imply that ^{13}C-$A\beta_{1-42}$ readily forms a cross-β structure even in the absence of an aqueous medium while $A\beta_{pE3-42}$ forms intramolecular β-hairpins and an α-helix. In aqueous (D_2O) buffer, both peptides adopt parallel intermolecular β-structure, as evidenced by the major amide I peaks at 1628 cm^{-1} for $A\beta_{pE3-42}$

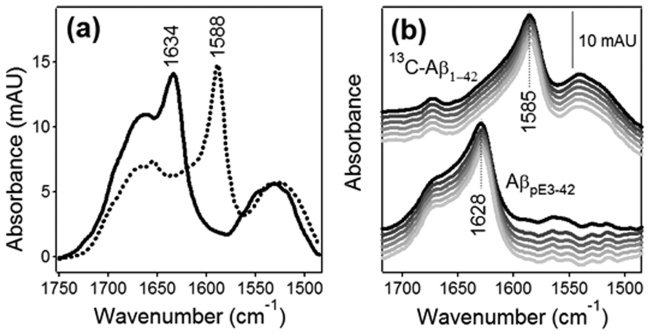

Figure 3. (a) FTIR spectra of $A\beta_{pE3-42}$ (solid) and uniformly ^{13}C-labeled $A\beta_{1-42}$ (dotted) dried from a 200 μM HFIP solution on a CaF_2 window. (b) FTIR spectra of the two peptides, as indicated, in 10 mM Na,K-phosphate in D_2O, pD 7.2. Decreasing line darkness corresponds to time of exposure of the peptides to the buffer for 10, 30, 50, 70, 90, and 120 min.

and 1585 cm^{-1} for ^{13}C-$A\beta_{1-42}$ (Figure 3b). However, the prominent component between 1680 and 1650 cm^{-1} in the spectra of $A\beta_{pE3-42}$ indicates that the pyroglutamylated peptide retains significant fractions of α-helical and turn structures. (The small peak in the spectra of ^{13}C-A_{1-42} at 1673 cm^{-1} is likely generated by trace amounts of trifluoroacetic acid usually present in synthetic peptide samples.)

The amide II spectral region provides additional structural information on proteins and peptides. Flexible secondary structures or open, solvent accessible tertiary structures undergo faster amide hydrogen/deuterium exchange resulting in reduction of the amide II band intensity around 1540 cm^{-1}.[45−47] A considerable amide II band is retained in the spectrum of ^{13}C-$A\beta_{1-42}$ after a 2 h exposure to D_2O while that of $A\beta_{pE3-42}$ is lost (Figure 3b), indicating $A\beta_{1-42}$ forms a rigid secondary structure and/or a tight, solvent-inaccessible tertiary structure, characteristic of a cross β-sheet structure,[10,11] while $A\beta_{pE3-42}$ has a more open tertiary structure and/or more flexible secondary structure.

It has been shown earlier that isotope-edited FTIR can be used to probe the intermolecular interactions of peptides.[43,44] In the case of closely spaced ^{13}C-labeled peptide units, through H-bonding or through space ^{13}C−^{13}C vibrational coupling between adjacent strands results in a lower frequency (∼1590−1594 cm^{-1}) amide I mode whereas ^{13}C−^{12}C coupling between labeled and unlabeled units generates higher frequency (∼1600−1604 cm^{-1}) components of enhanced intensity.[20,48,49] FTIR studies were conducted on combined ^{13}C-$A\beta_{1-42}$ and unlabeled $A\beta_{pE3-42}$ to probe (a) the intermolecular interactions and (b) mutual structural effects of the peptides. Since pE-Aβ in AD brain can constitute up to 50% of total Aβ,[34,35] we studied $A\beta_{pE3-42}/^{13}$C-$A\beta_{1-42}$ samples at 10% and 50% molar fractions of $A\beta_{pE3-42}$. Data of Figure 4 indicate that the β-sheet peak of ^{13}C-$A\beta_{1-42}$ at 1585 cm^{-1} up-shifts by 3 and 10 cm^{-1} in the presence of 10% and 50% pE-Aβ, respectively, while the β-sheet peak of $A\beta_{pE3-42}$ at 1626−1628 cm^{-1} up-shifts by 10 and 4 cm^{-1} in the presence of 90% and 50% ^{13}C-$A\beta_{1-42}$, respectively, indicating strong interactions and vibrational couplings between the two peptides. Thus, $A\beta_{pE3-42}$ and $A\beta_{1-42}$ form a mixed β-sheet structure with tight intermolecular interactions.

Next, we tested the emerging hypothesis that the pyroglutamylated peptide is able to modulate the structure of the unmodified Aβ during amyloid fibril formation. To assess early structural events in aggregation, combinations of HFIP

dx.doi.org/10.1021/jp412743s | J. Phys. Chem. B 2014, 118, 5637−5643

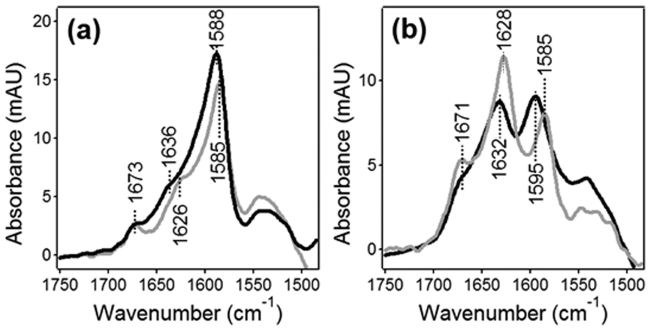

Figure 4. FTIR spectra of A$\beta_{pE3\text{-}42}$ and ^{13}C-Aβ_{1-42} combined at 1:9 (a) and 1:1 (b) molar ratios, incubated in a D_2O-based phosphate buffer (pD 7.2) for 2 h, at a total peptide concentration of 100 μM. Black and gray lines are the experimental spectra obtained on the two peptides combined in one sample and the weighted sums of individual spectra, respectively. The weighted sums were obtained as $A = \sum f_i A_i$, where f_i is the molar fraction and A_i is the absorbance spectrum of each individual peptide measured separately.

solutions of A$\beta_{pE3\text{-}42}$ and ^{13}C-Aβ_{1-42} were dried on a FTIR CaF_2 window followed by collection of spectra while the sample was allowed to absorb atmospheric humidity. Figure 5a shows the spectra of A$\beta_{pE3\text{-}42}$ and ^{13}C-Aβ_{1-42} combined at 1:9 molar ratio in a wide spectral range. The 1700−1500 cm^{-1} region corresponds to the amide I and amide II modes and reflects the peptides' secondary and dynamic structure whereas the signal in the 3450−3150 cm^{-1} region results from the amide A and H_2O stretching modes.[45−47] Spectra shown in gray and black solid lines in Figure 5a and b were collected on a sample that was dried by desiccation and exposed to the atmosphere for 10 and 20 min, respectively. The peptides absorb atmospheric humidity, which results in an increase in the H_2O stretching band around 3270 cm^{-1}. Nominal hydration causes conformational transitions in both peptides and corresponding spectral changes in the amide I region, shown in Figure 5b. At a 1:9 A$\beta_{pE3\text{-}42}$/^{13}C-Aβ_{1-42} molar ratio, the amide I band is dominated by the spectral features of the latter peptide, i.e. α-helical and β-sheet components at 1617 and 1592 cm^{-1}, respectively (Figure 5b). The broad band around 1655 cm^{-1} evidently results from the overlapped α-helical mode of A$\beta_{pE3\text{-}42}$ and the turn structures of ^{13}C-Aβ_{1-42}. As the sample absorbs atmospheric moisture, ^{13}C-Aβ_{1-42} undergoes α-to-β transition (intensity transfer from 1617 to 1592 cm^{-1}, cf. gray and black solid lines in Figure 5b). However, a more humid 1:9 mixture (black solid line) contains less β-sheet and more α-helix than expected without interaction between the two peptides (the weighted sum of individual spectra shown in a dotted line). These and above data suggest that pE-Aβ slows down cross β-sheet formation in Aβ by direct intermolecular interactions.

Moreover, at 1:1 molar combination, pE-Aβ reverses the cross-β structure and hence fibrillization of Aβ. As shown in Figure 5c, in the presence of 50% pE-Aβ, the intermolecular β-sheet peak of ^{13}C-Aβ_{1-42} shifts from 1588 to 1595 cm^{-1} (cf. dotted and gray spectra), indicating strong interaction between the two peptides. (In the presence of only 10% A$\beta_{pE\text{-}42}$, a smaller shift from 1588 to 1592 cm^{-1} is observed, Figure 5b.) In the presence of an equimolar amount of A$\beta_{pE3\text{-}42}$, there is no α-helix to β-sheet conversion of ^{13}C-Aβ_{1-42} over time, as seen by the similar signal intensity at 1617 cm^{-1} in gray and black solid spectra in Figure 5c. Most importantly, A$\beta_{pE3\text{-}42}$ causes a strong reduction of the intermolecular β-sheet signal of ^{13}C-Aβ_{1-42} at 1595 cm^{-1} during longer coincubation (cf. gray and black solid spectra in Figure 5c) paralleled with increased intensity around 1658 cm^{-1}. The spectra of the combination (gray and black solid lines in Figure 5c) indicate an increase in α-helical structure (signals at 1658 and 1617 cm^{-1}) and a decrease in β-sheet structure (signals at 1634 and 1585−1588 cm^{-1}) in both peptides as compared to the weighted sum of individual spectra (dotted line in Figure 5c). Although the component at 1658 cm^{-1} might partially result from turn structures in addition to the α-helix in A$\beta_{pE3\text{-}42}$, these data identify prominent mutual conformational effects of the two peptides; pE-Aβ at 10% delays cross β-sheet formation and hence fibrillization and at 50% reverses the cross β-sheet structure formation of Aβ.

4. DISCUSSION

Our data identify significant differences between A$\beta_{pE3\text{-}42}$ and Aβ_{1-42} at the levels of morphology as well as secondary and tertiary structures. At the initial stages of fibrillogenesis, the pyroglutamylated A$\beta_{pE3\text{-}42}$ peptide forms more prefibrillar aggregates, apparently due to its increased hydrophobicity, and it undergoes fibril elongation slower than the unmodified Aβ_{1-42} peptide (Figure 1a,b), in agreement with earlier data.[31] Retardation of fibrillization appears to be imparted to Aβ_{1-42} even at low molar contents of A$\beta_{pE3\text{-}42}$ (Figure 1c). CD data indicate augmented α-helical and diminished β-sheet propensity of A$\beta_{pE3\text{-}42}$, which is transmitted to the mixed assemblies (Figure 2). FTIR indicates that the unmodified peptide readily forms a tightly packed intermolecular β-sheet, while pE-Aβ

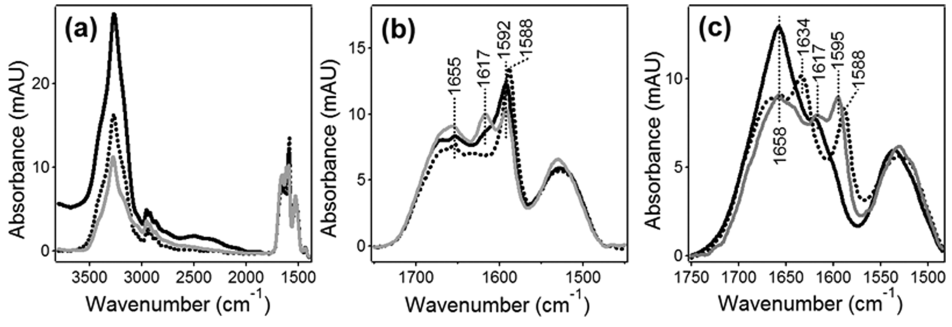

Figure 5. FTIR spectra of A$\beta_{pE3\text{-}42}$ and uniformly ^{13}C-labeled Aβ_{1-42} at 1:9 molar ratio (a and b) and 1:1 molar ratio (c). Gray and black solid lines are experimental spectra of a sample prepared in HFIP, followed by solvent removal by desiccation and exposure to atmosphere for 10 and 20 min, respectively. The dotted spectrum is the weighted sum of the spectra of each peptide measured individually, exposed to the atmosphere for 15 min. Construction of the weighted sum spectra is described under Figure 4. Panel b is a zoom-in into the amide I/II region of spectra shown in panel a.

dx.doi.org/10.1021/jp412743s | J. Phys. Chem. B 2014, 118, 5637−5643

forms a less compact β-structure and contains more α-helix and turn structures than Aβ (Figure 3). Furthermore, the pyroglutamylated peptide not only exhibits a significantly lower tendency to form a β-sheet structure but also inhibits cross β-sheet formation in the unmodified peptide through direct interactions (Figures 4 and 5). These structural transitions occur rapidly upon hydration, but they can be captured when the peptides undergo nominal hydration by exposure to atmospheric humidity. These conditions are both technically beneficial and meaningful because the fibrils formed by $A\beta_{1-40}$ were shown to contain an extremely low fraction of water, i.e., an average of 1.2 water molecules per β-strand.[50] Significant retention of the amide II band in the spectrum of $A\beta_{1-42}$ in a D_2O-based buffer (Figure 3b) is in line with this finding. Furthermore, the rapid loss of the amide II band of $A\beta_{pE3-42}$ upon exposure to D_2O indicates a more flexible secondary and/or a more open tertiary structure of the pyroglutamylated peptide.

If pE-Aβ eventually forms fibrils that contain β-sheet structure, even though different from the fibrils formed by unmodified Aβ, why do the intermediate structural steps matter? The answer is that the oligomeric, prefibrillar assemblies of Aβ that adopt still poorly characterized "pathological conformation" are the most toxic species.[51] For example, the secreted pool of Aβ oligomers exerts its toxic effect partly by binding to a set of receptors, including the insulin receptor that recognizes an α-helical ligand.[51] Intracellular oligomers bind to the mitochondrial or endoplasmic reticulum proteins and cause cell damage through oxidative stress or calcium dysregulation before they are secreted.[52,53] Since the cytotoxic effect is exerted before formation of the extracellular deposits, chracterizaton of the intermediate "pathological conformations" is crucial.

The structural impact of pE-Aβ on the unmodified peptide even at low molar content (10%) is indicative of a prion-like effect. The pE-Aβ peptide tightly interacts with Aβ, as indicated by efficient $^{12}C-^{13}C$ vibrational coupling (Figures 4 and 5), and thereby transmits the specific structural features to the unmodified peptide. Data of Figures 2−5 strongly imply that this specific structure is rich in α-helix as opposed to β-sheet. This effect takes place even at 10% pE-Aβ, when pE-Aβ molecules cannot simultaneously interact with a large excess of unmodified Aβ. We therefore propose that once the structural transition occurs in the unmodified Aβ molecule by its interaction with pE-Aβ, it acquires the capability to further transmit the altered structure to other Aβ peptides by direct interaction. This prion-like conformational effect of pE-Aβ may eventually shift the overall path of peptide aggregation toward formation of hypertoxic, lower molecular weight aggregates of partial α-helical structure and thus suppress formation of less toxic cross β-sheet fibrils.

AUTHOR INFORMATION

Corresponding Author

*E-mail: statulia@ucf.edu. Tel.: +1-407-823-6941. Fax: +1-407-823-5112.

Notes

The authors declare no competing financial interest.

ACKNOWLEDGMENTS

This work was partially supported by NIH Grant 1R03AI097591 to S.A.T, a SEED grant from the College of Sciences of the University of Central Florida to S.A.T., and the Air Force Office of Scientific Research Young Investigator Award FA9550-13-1-0150 to B.C. The ICBR Proteomics Core Facility of the University of Florida is acknowledged for mass-spec characterization of the peptides.

REFERENCES

(1) Hardy, J.; Allsop, D. Amyloid Deposition as the Central Event in the Aetiology of Alzheimer's Disease. *Trends Pharmacol. Sci.* **1991**, *12*, 383−388.

(2) Pike, C. J.; Burdick, D.; Walencewicz, A. J.; Glabe, C. G.; Cotman, C. W. Neurodegeneration Induced by β-Amyloid Peptides *in vitro*: The Role of Peptide Assembly State. *J. Neurosci.* **1993**, *13*, 1676−1687.

(3) Hardy, J.; Selkoe, D. J. The Amyloid Hypothesis of Alzheimer's Disease: Progress and Problems on the Road to Therapeutics. *Science* **2002**, *297*, 353−356.

(4) Kirkitadze, M. D.; Bitan, G.; Teplow, D. B. Paradigm Shifts in Alzheimer's Disease and Other Neurodegenerative Disorders: The Emerging Role of Oligomeric Assemblies. *J. Neurosci. Res.* **2002**, *69*, 567−577.

(5) Klein, W. L.; Stine, W. B.; Teplow, D. B. Small Assemblies of Unmodified Amyloid β-Protein Are the Proximate Neurotoxin in Alzheimer's Disease. *Neurobiol. Aging* **2004**, *25*, 569−580.

(6) Bernstein, S. L.; Dupuis, N. F.; Lazo, N. D.; Wyttenbach, T.; Condron, M. M.; Bitan, G.; Teplow, D. B.; Shea, J. E.; Ruotolo, B. T.; Robinson, C. V.; Bowers, M. T. Amyloid-β Protein Oligomerization and the Importance of Tetramers and Dodecamers in the Aetiology of Alzheimer's Disease. *Nat. Chem.* **2009**, *1*, 326−331.

(7) Masters, C. L.; Selkoe, D. J. Biochemistry of Amyloid β-Protein and Amyloid Deposits in Alzheimer Disease. *Cold Spring Harb. Perspect. Med.* **2012**, *2* (a006262), 1−24.

(8) Benilova, I.; Karran, E.; De Strooper, B. The Toxic Aβ Oligomer and Alzheimer's Disease: An Emperor in Need of Clothes. *Nat. Neurosci.* **2012**, *15*, 349−357.

(9) Tomaselli, S.; Esposito, V.; Vangone, P.; van Nuland, N. A.; Bonvin, A. M.; Guerrini, R.; Tancredi, T.; Temussi, P. A.; Picone, D. The α-to-β Conformational Transition of Alzheimer's Aβ-(1-42) Peptide in Aqueous Media is Reversible: A Step by Step Conformational Analysis Suggests the Location of β Conformation Seeding. *ChemBioChem* **2006**, *7*, 257−267.

(10) Eanes, E. D.; Glenner, G. G. X-Ray Diffraction Studies on Amyloid Filaments. *J. Histochem. Cytochem.* **1968**, *16*, 673−677.

(11) Kirschner, D. A.; Inouye, H.; Duffy, L. K.; Sinclair, A.; Lind, M.; Selkoe, D. J. Synthetic Peptide Homologous to Beta Protein from Alzheimer Disease Forms Amyloid-Like Fibrils *in vitro*. *Proc. Natl. Acad. Sci. U.S.A.* **1987**, *84*, 6953−6957.

(12) Petkova, A. T.; Buntkowsky, G.; Dyda, F.; Leapman, R. D.; Yau, W. M.; Tycko, R. Solid State NMR Reveals a pH-Dependent Antiparallel β-Sheet Registry in Fibrils Formed by a β-Amyloid Peptide. *J. Mol. Biol.* **2004**, *335*, 247−260.

(13) Chaney, M. O.; Webster, S. D.; Kuo, Y. M.; Roher, A. E. Molecular Modeling of the Aβ1-42 Peptide from Alzheimer's Disease. *Protein Eng.* **1998**, *11*, 761−767.

(14) Petkova, A. T.; Ishii, Y.; Balbach, J. J.; Antzutkin, O. N.; Leapman, R. D.; Delaglio, F.; Tycko, R. A Structural Model for Alzheimer's β-Amyloid Fibrils Based on Experimental Constraints from Solid State NMR. *Proc. Natl. Acad. Sci. U.S.A.* **2002**, *99*, 16742−16747.

(15) Paravastu, A. K.; Leapman, R. D.; Yau, W. M.; Tycko, R. Molecular Structural Basis for Polymorphism in Alzheimer's β-Amyloid Fibrils. *Proc. Natl. Acad. Sci. U.S.A.* **2008**, *105*, 18349−18354.

(16) Goldsbury, C. S.; Wirtz, S.; Müller, S. A.; Sunderji, S.; Wicki, P.; Aebi, U.; Frey, P. Studies on the *in vitro* Assembly of Aβ 1−40: Implications for the Search for Aβ Fibril Formation Inhibitors. *J. Struct. Biol.* **2000**, *130*, 217−231.

(17) Török, M.; Milton, S.; Kayed, R.; Wu, P.; McIntire, T.; Glabe, C. G.; Langen, R. Structural and Dynamic Features of Alzheimer's Aβ

Peptide in Amyloid Fibrils Studied by Site-Directed Spin Labeling. *J. Biol. Chem.* **2002**, *277*, 40810−40815.
(18) Lührs, T.; Ritter, C.; Adrian, M.; Riek-Loher, D.; Bohrmann, B.; Döbeli, H.; Schubert, D.; Riek, R. 3D Structure of Alzheimer's Amyloid-$\beta_{1\text{-}42}$ Fibrils. *Proc. Natl. Acad. Sci. U.S.A.* **2005**, *102*, 17342−17347.
(19) Kim, Y. S.; Liu, L.; Axelsen, P. H.; Hochstrasser, R. M. Two-Dimensional Infrared Spectra of Isotopically Diluted Amyloid Fibrils from Aβ40. *Proc. Natl. Acad. Sci. U.S.A.* **2008**, *105*, 7720−7725.
(20) Paul, C.; Axelsen, P. H. β Sheet Structure in Amyloid β Fibrils and Vibrational Dipolar Coupling. *J. Am. Chem. Soc.* **2005**, *127*, 5754−5755.
(21) Cerf, E.; Sarroukh, R.; Tamamizu-Kato, S.; Breydo, L.; Derclaye, S.; Dufrêne, Y. F.; Narayanaswami, V.; Goormaghtigh, E.; Ruysschaert, J. M.; Raussens, V. Antiparallel β-Sheet: A Signature Structure of the Oligomeric Amyloid β-Peptide. *Biochem. J.* **2009**, *421*, 415−423.
(22) Schilling, S.; Lauber, T.; Schaupp, M.; Manhart, S.; Scheel, E.; Böhm, G.; Demuth, H. U. On the Seeding and Oligomerization of pGlu-Amyloid Peptides (*in vitro*). *Biochemistry* **2006**, *45*, 12393−12399.
(23) Schlenzig, D.; Manhart, S.; Cinar, Y.; Kleinschmidt, M.; Hause, G.; Willbold, D.; Funke, S. A.; Schilling, S.; Demuth, H. U. Pyroglutamate Formation Influences Solubility and Amyloidogenicity of Amyloid Peptides. *Biochemistry* **2009**, *48*, 7072−7078.
(24) Schlenzig, D.; Rönicke, R.; Cynis, H.; Ludwig, H. H.; Scheel, E.; Reymann, K.; Saido, T.; Hause, G.; Schilling, S.; Demuth, H. U. N-Terminal Pyroglutamate Formation of Aβ38 and Aβ40 Enforces Oligomer Formation and Potency To Disrupt Hippocampal Long-Term Potentiation. *J. Neurochem.* **2012**, *121*, 774−784.
(25) He, W.; Barrow, C. J. The Aβ 3-Pyroglutamyl and 11-Pyroglutamyl Peptides Found in Senile Plaque Have Greater β-Sheet Forming and Aggregation Propensities *in vitro* than Full-Length Aβ. *Biochemistry* **1999**, *38*, 10871−10877.
(26) Wirths, O.; Erck, C.; Martens, H.; Harmeier, A.; Geumann, C.; Jawhar, S.; Kumar, S.; Multhaup, G.; Walter, J.; Ingelsson, M.; Degerman-Gunnarsson, M.; Kalimo, H.; Huitinga, I.; Lannfelt, L.; Bayer, T. A. Identification of Low Molecular Weight Pyroglutamate Aβ Oligomers in Alzheimer Disease: A Novel Tool for Therapy and Diagnosis. *J. Biol. Chem.* **2010**, *285*, 41517−41524.
(27) Nussbaum, J. M.; Schilling, S.; Cynis, H.; Silva, A.; Swanson, E.; Wangsanut, T.; Tayler, K.; Wiltgen, B.; Hatami, A.; Rönicke, R.; Reymann, K.; Hutter-Paier, B.; Alexandru, A.; Jagla, W.; Graubner, S.; Glabe, C. G.; Demuth, H. U.; Bloom, G. S. Prion-Like Behaviour and Tau-Dependent Cytotoxicity of Pyroglutamylated Amyloid-β. *Nature* **2012**, *485*, 651−655.
(28) Russo, C.; Violani, E.; Salis, S.; Venezia, V.; Dolcini, V.; Damonte, G.; Benatti, U.; D'Arrigo, C.; Patrone, E.; Carlo, P.; Schettini, G. Pyroglutamate-Modified Amyloid β-Peptides − Aβ$N3_{pE}$ − Strongly Affect Cultured Neuron and Astrocyte Survival. *J. Neurochem.* **2002**, *82*, 1480−1489.
(29) Sun, N.; Hartmann, R.; Lecher, J.; Stoldt, M.; Funke, S. A.; Gremer, L.; Ludwig, H. H.; Demuth, H. U.; Kleinschmidt, M.; Willbold, D. Structural Analysis of the Pyroglutamate-Modified Isoform of the Alzheimer's Disease-Related Amyloid-β Using NMR Spectroscopy. *J. Pept. Sci.* **2012**, *18*, 691−695.
(30) Tekirian, T. L.; Yang, A. Y.; Glabe, C.; Geddes, J. W. Toxicity of Pyroglutaminated Amyloid β-Peptides 3pE-40 and -42 is Similar to that of Aβ 1-40 and -42. *J. Neurochem.* **1999**, *73*, 1584−1589.
(31) Sanders, H. M.; Lust, R.; Teller, J. K. Amyloid-β Peptide Aβp3-42 Affects Early Aggregation of Full-Length Aβ1-42. *Peptides* **2009**, *30*, 849−854.
(32) Petkova, A. T.; Leapman, R. D.; Guo, Z.; Yau, W. M.; Mattson, M. P.; Tycko, R. Self-Propagating, Molecular-Level Polymorphism in Alzheimer's β-Amyloid Fibrils. *Science* **2005**, *307*, 262−265.
(33) Jeong, J. S.; Ansaloni, A.; Mezzenga, R.; Lashuel, H. A.; Dietler, G. Novel Mechanistic Insight into the Molecular Basis of Amyloid Polymorphism and Secondary Nucleation during Amyloid Formation. *J. Mol. Biol.* **2013**, *425*, 1765−1781.
(34) Saido, T. C.; Iwatsubo, T.; Mann, D. M.; Shimada, H.; Ihara, Y.; Kawashima, S. Dominant and Differential Deposition of Distinct β-Amyloid Peptide Species, Aβ$N3_{pE}$, in Senile Plaques. *Neuron* **1995**, *14*, 457−466.
(35) Wu, G.; Miller, R. A.; Connolly, B.; Marcus, J.; Renger, J.; Savage, M. J. Pyroglutamate-Modified Amyloid-β Protein Demonstrates Similar Properties in an Alzheimer's Disease Familial Mutant Knock-In Mouse and Alzheimer's Disease Brain. *Neurodegener. Dis.* **2013**, *Oct 23*, 1−14.
(36) Nilsson, M. R. Techniques To Study Amyloid Fibril Formation in vitro. *Methods* **2004**, *34*, 151−160.
(37) Tatulian, S. A.; Garg, G.; Nemec, K. N.; Chen, B.; Khaled, A. R. Molecular Basis for Membrane Pore Formation by Bax Protein Carboxyl Terminus. *Biochemistry* **2012**, *51*, 9406−9419.
(38) D'Arrigo, C.; Tabaton, M.; Perico, A. N-Terminal Truncated Pyroglutamyl β Amyloid Peptide Aβpy3-42 Shows a Faster Aggregation Kinetics than the Full-Length Aβ1-42. *Biopolymers* **2009**, *91*, 861−873.
(39) Galante, D.; Corsaro, A.; Florio, T.; Vella, S.; Pagano, A.; Sbrana, F.; Vassalli, M.; Perico, A.; D'Arrigo, C. Differential Toxicity, Conformation and Morphology of Typical Initial Aggregation States of Aβ1-42 and Aβpy3-42 Beta-Amyloids. *Int. J. Biochem. Cell Biol.* **2012**, *44*, 2085−2093.
(40) Sreerama, N.; Woody, R. W. Circular Dichroism of Peptides and Proteins. In *Circular Dichroism: Principles and Applications*; Berova, N., Nakanishi, K., Woody, R. W., Eds.; John Wiley & Sons: Hoboken, NJ, 2000; pp 601−620.
(41) Bakshi, K.; Liyanage, M. R.; Volkin, D. B.; Middaugh, C. R. Circular Dichroism of Peptides. *Methods Mol. Biol.* **2014**, *1088*, 247−253.
(42) Sreerama, N.; Venyaminov, S. Y.; Woody, R. W. Estimation of the Number of α-Helical and β-Strand Segments in Proteins Using Circular Dichroism Spectroscopy. *Protein Sci.* **1999**, *8*, 370−380.
(43) Decatur, S. M. Elucidation of Residue-Level Structure and Dynamics of Polypeptides via Isotope-Edited Infrared Spectroscopy. *Acc. Chem. Res.* **2006**, *39*, 169−175.
(44) Haris, P. I. Probing Protein-Protein Interaction in Biomembranes Using Fourier Transform Infrared Spectroscopy. *Biochim. Biophys. Acta* **2013**, *1828*, 2265−2271.
(45) Tatulian, S. A. Structural Characterization of Membrane Proteins and Peptides by FTIR and ATR-FTIR Spectroscopy. *Methods Mol. Biol.* **2013**, *974*, 177−218.
(46) Goormaghtigh, E.; Cabiaux, V.; Ruysschaert, J. M. Determination of Soluble and Membrane Protein Structure by Fourier Transform Infrared Spectroscopy. III. Secondary Structures. *Subcell. Biochem.* **1994**, *23*, 405−450.
(47) Bakshi, K.; Liyanage, M. R.; Volkin, D. B.; Middaugh, C. R. Fourier Transform Infrared Spectroscopy of Peptides. *Methods Mol. Biol.* **2014**, *1088*, 255−269.
(48) Petty, S. A.; Decatur, S. M. Experimental Evidence for the Reorganization of β-Strands within Aggregates of the $A\beta_{16-22}$ Peptide. *J. Am. Chem. Soc.* **2005**, *127*, 13488−13489.
(49) Petty, S. A.; Decatur, S. M. Intersheet Rearrangement of Polypeptides during Nucleation of β-Sheet Aggregates. *Proc. Natl. Acad. Sci. U.S.A.* **2005**, *102*, 14272−14277.
(50) Kim, Y. S.; Liu, L.; Axelsen, P. H.; Hochstrasser, R. M. 2D IR Provides Evidence for Mobile Water Molecules in β-Amyloid Fibrils. *Proc. Natl. Acad. Sci. U.S.A.* **2009**, *106*, 17751−17756.
(51) Benilova, I.; De Strooper, B. Promiscuous Alzheimer's Amyloid: Yet Another Partner. *Science* **2013**, *341*, 1354−1355.
(52) Deshpande, A.; Mina, E.; Glabe, C.; Busciglio, J. Different Conformations of Amyloid β Induce Neurotoxicity by Distinct Mechanisms in Human Cortical Neurons. *J. Neurosci.* **2006**, *26*, 6011−6018.
(53) Manczak, M.; Calkins, M. J.; Reddy, P. H. Impaired Mitochondrial Dynamics and Abnormal Interaction of Amyloid β with Mitochondrial Protein Drp1 in Neurons from Patients with Alzheimer's Disease: Implications for Neuronal Damage. *Hum. Mol. Genet.* **2011**, *20*, 2495−2509.